Pre-transition Oxide Characterization of Zirconium Alloy Cladding on the Zinc Injection and the High Dissolved Hydrogen Condition

Sungyu Kim[1], Taeho Kim[2], Ji Hyun Kim[2], Chi Bum Bahn[1*]

[1] *School of Mechanical Engineering, Pusan National University, Busan 46241, Republic of Korea*
[2] *Department of Nuclear Engineering, School of Mechanical, Aerospace and Nuclear Engineering, Ulsan National Institute of Science and Technology (UNIST), Ulsan 44919, Republic of Korea*
** Corresponding author: bahn@pusan.ac.kr*

ABSTRACT: *In order to evaluate any possible effects of Zn and dissolved hydrogen concentrations on the pre-transition oxide formation, Zr-Nb-Sn tube samples were exposed to simulating primary water chemistry conditions by varying Zn (30 ppb) or dissolved hydrogen (30 to 50 cc/kg) concentrations. The pre-transition oxide formed on Zr-Nb-Sn tube samples was microscopically examined by using scanning transmission electron microscopy with sectioned samples prepared by a focused ion beam technique. Microstructure analysis indicated that there was no noticeable change in the microstructure of the oxide corresponding to the water chemistry change within the test duration of 100 days (pre-transition stage), and there was no significant difference in the thickness of the oxide layer. Equiaxed grains with nano-size porosities along the grain boundaries and micro-cracks were dominant near the water/oxide interface, regardless of water chemistry conditions. As the metal/oxide interface was approached, the number of pore tended to decrease. In the case of high hydrogen concentration (50 cc/kg), there was no significant difference in the corrosion of the oxide compared with the 30 cc/kg hydrogen concentration condition. From the perspective of OH^- ion diffusion and porosity formation, the absence of noticeable effects was discussed further.*

KEYWORDS: *Oxide, Pre-transition, Primary Water, Transmission Electron Microscopy, Porosity*

I. Introduction

Corrosion of the zirconium fuel cladding is known to limit the lifetime and cycle of the reloading fuel in the reactor. Therefore, extensive research has been conducted to better understand the mechanism of corrosion and damages of zirconium fuel cladding. However, there is still no clear understanding of oxide growth mechanism related to cladding integrity. Corrosion kinetics of zirconium alloy has been widely known to consist of three stages: pre-transition, transitory, and post-transition (Ref. 1).

Other researchers recently suggested that interconnection of porosity from the water/oxide interface to the metal/oxide interface is a key mechanism for oxide transition (Ref. 2). Bossis et al. reported a porous outer layer in a pre-transition oxide analyzed by a secondary ion mass spectrometry (SIMS) and an electrical impedance spectroscopy (EIS) (Ref. 3). Cox et al. anticipated that porosity provides connected paths between the external oxidizing medium and the underlying metal (Ref. 4). Gong et al. reported nano-pores in strings formed on Zr-Nb-Y alloy and N18 alloy (Zr – 0.39Nb – 0.93Sn – 0.31Fe – 0.08Cr – 0.048O, wt.%) at grain boundaries and they suggested that the initiation mechanism of porosity is due to the Kirkendall effect (Ref. 5).

Earlier studies on Zr alloy corrosion did not pay much attention to the effects of water chemistry. Zn injection and adjusting the dissolved hydrogen concentration in a pressurized water reactor operating as a primary water chemistry control have been considered as measures to alleviate the radiation build-up and reduce cracking in a nickel-based alloy (Ref. 6~10). However, the effect of oxidation on the nuclear fuel cladding, especially in a Pressurized Water Reactor (PWR) has not been systematically studied yet.

The main purpose of this study is to investigate the microstructure of the oxide layer as well as the effects of Zn injection and high hydrogen concentrations on the oxide corrosion. To evaluate the possible influence on the pre-transition oxide form, Zr-Nb-Sn tube specimens were exposed to simulated primary water chemistry conditions by varying Zn and dissolved hydrogen concentrations. The comparison results can provide insight on the corrosion mechanism of zirconium fuel cladding and the effects of zinc injection and high hydrogen concentrations.

II. Experimental Procedure

Zr-Nb-Sn alloy tube has been oxidized in an autoclave connected to a recirculation water loop at 360 ℃ and 20 MPa for 300 hours, 50 days, and 100 days under a simulated primary water chemistry condition (pure H_2O with dissolved hydrogen of 30 cc/kg, dissolved oxygen of 0~5 ppb, 2 ppm Li^+ as LiOH and 1200 ppm B^{3+} as H_3BO_3). Dissolved hydrogen and dissolved oxygen were measured by dissolved gas meters. The pressure difference between interior and exterior of the cladding sample was maintained at 11.7 MPa by pressurizing argon gas to 4.56 MPa at room temperature during the exposure in the recirculation loop in order to simulate the compressive stress condition in the actual fuel cladding. For experiments with high hydrogen concentrations, the concentrations were increased to 50 cc/kg from 30 cc/kg and 30 ppb of Zn was injected to test the Zn injection effect on sample oxidation. The dimensions of the test samples were 9.5 mm in outer diameter, 8.3 mm in inner diameter, and 0.6 mm in thickness with a length of 130 mm. The nominal chemical compositions of the test sample and the Zr-0.66Sn alloy sample (Ref. 11) are shown in Table 1 for comparison with the thickness results. All tests were performed without consideration of heat flux and chalk river unidentified deposits (CRUD).

After an immersion corrosion test, a protective coating of platinum was deposited on the oxide surface, and then in-situ lift-out Focused ion beam (FIB) sectioning was carried out with a FEI Quanta 3D FEG instrument operated at 2-30 kV, with currents between 1 pA and 65 nA to prepare Transmission electron microscopy (TEM) thin foils for microstructure analysis in the oxide layer. Cs-corrected scanning transmission electron microscopy (STEM) observations were carried out with a JEOL JEM-ARM200F operated at 200 kV. The composition of the precipitates was characterized by energy dispersive x-ray spectroscopy (EDS) elemental mapping. The thickness of the oxide layer was determined by STEM images. In case of the sample corroded for 100 days having an increased interface roughness, the thickness was determined by scanning electron microscopy (SEM) images to analyze the large area. SEM image measurement was carried out with a ZEISS SUPRA™ 40. Corrosion of the zirconium fuel cladding is known to limit the lifetime and cycle of the reloading fuel in the reactor. Therefore, extensive research has been conducted to better understand the mechanism of corrosion and damages of zirconium fuel cladding.

Table 1. Chemical composition of the materials

	Nb	Sn	Fe	O	C	N	Hf	Zr
Zr-Nb-Sn alloy	0.96	0.76	0.18	0.62	0.1	0.03	0.002	Bal.
Wei et al. (Ref. 11)	0.91	0.66	0.09	-	-	-	-	Bal.
(Unit: wt %)								

III. Results & Discussion

III. 1. Thickness measurement

Oxide layer thickness was measured for the reference condition, high hydrogen concentration, and Zn injection over varying time periods. For 300 hours and 50 days corroded- samples, the oxide thickness was measured by STEM images. However, in the case of 100 days corroded- samples, when the metal/oxide interface became more irregular, the oxide thickness was measured by SEM images for a wider range of measurements. Based on the measured oxide thickness data as a function of time in all water chemistry conditions, Zn injection and high hydrogen concentration are not likely to

significantly affect the oxide growth kinetics. The results of oxide thickness of tested samples were compared with earlier data (Ref. 11). The experimental environment of the other researchers is similar to our study (only difference in H_3BO_3 concentration), but the experiment was performed with a static autoclave. The chemical composition of the samples used in the experiment is slightly different. As shown in Fig. 1, the difference of oxide thickness between the two experiments was less than 0.5 μm, and the overall thickness variation tendency is similar to each other. Therefore, the absolute thickness value difference appears to be caused by the difference between experimental conditions and chemical compositions of samples.

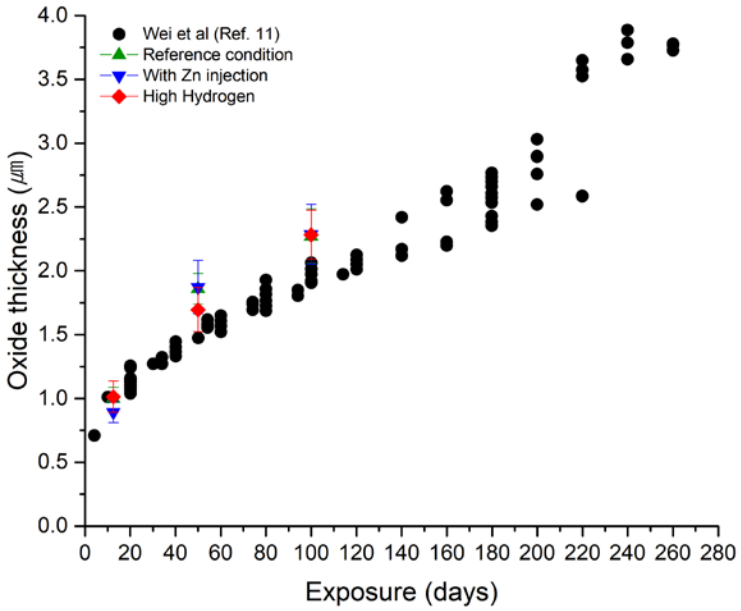

Fig. 1. Comparison of the average oxide thickness under each condition and with another study (Ref. 11). The values of the oxide thickness of 100 days corroded- samples were measured by SEM, and the 300 hours and 50 days corroded sample's oxide thickness were measured by STEM image.

III. 2. Porosity analysis

Figure 2 shows that the porosity formed in the outer part of the oxide in the form of being connected around the grains. These interlinked porosities existed not only at the equiaxed grain boundaries, but also in the columnar grain boundaries that existed at the center of the oxide layer. Where the grains are facing each other, a triangular micro-crack is formed. The density of porosity is the highest at the top of the oxide where corrosion begins, and decreases as it goes down to the metal/oxide interface. As the corrosion time increases from 300 hours to 100 days, the porous region, in which porosity is observed, increases gradually. This tendency is observed not only in the reference condition but also during Zn injection and at high hydrogen concentrations. It could be concluded that the interlinked porosity formed at the water/oxide, interface becomes wider when the porous region expands in the metal/oxide interface direction as the oxide layer is corroded. The disconnected porosity at the metal/oxide interface changes into a continuous form (interlinked porosity). External elements could diffuse easily along the passage formed by the interlinked porosity, which affects the corrosion kinetics.

To prove that the observed porosity in STEM is indeed the vacant area, additional analysis was conducted. The TEM under-focusing technique was used for further analysis of the porosity observed in the porous region. In the case of a general TEM, the object is analyzed using the interference effect of the wave using a beam having a size of 1 mm. At this time, there is a large phase shift in the place depending on whether the object to be analyzed exists or not, which is called a Fresnel Fringe (Ref. 12). We used the under focusing technique to maximize the Fresnel Fringe effect and show that the porosities observed in the STEM dark field are actually vacant areas. A comparison of the STEM dark field image and the TEM under-focusing image at the same location is shown in Fig. 3. The porosity and micro-cracks observed in the STEM dark field image were also observed in the TEM under-focusing image at the same location, and the pores near the oxide/water

interface were formed as interlinked porosity around the equiaxed grain. The density of porosity tended to decrease from the water/oxide interface toward the metal/oxide interface, which was also observed in the TEM under-focus image as in the STEM dark field image. From these comparisons, it was confirmed that the pores observed on the STEM image from the water/oxide interface to the middle of oxide layer (porous region) are vacant areas indeed.

By analysis conducting STEM and TEM under-focusing techniques, we found that Zn injection and high hydrogen concentrations did not significantly affect the microstructure of oxide layers, while comparing the oxide thickness showed that neither condition affected the corrosion of the oxide layer. Analysis for the porous region suggests that the path formed by interlinked porosity along the grain boundary may allow oxygen to penetrate easily and ultimately trigger the transition. From the perspective of the interlinked porosity, there were no noticeable effects of Zn injection and high dissolved hydrogen concentration conditions suggest that Zn adsorbs only on the Zr oxide surface and is not involved in the porosity formation process. Similarly, it is unlikely that the increase in the dissolved hydrogen concentration can affect the porosity formation mechanism at least within the range of experimental conditions we tested.

IV. Porosity formation mechanism & Post-transition

The answer to why the transition in corrosion kinetic occurs is still being actively discussed. Corrosion of the oxide layer is may closely related to the formation mechanism of porosity observed in this study. However, the cause of the formation of these nano-scale porosities at the grain boundaries is not yet clear. Several porosity formation mechanisms are available. It has been claimed that nano porosity can be formed by the Kirkendall effect (Ref. 12), which has been criticized by other researchers (Ref. 13). Another possible mechanism stems from the hydrothermal degradation of tetragonal zirconia polycrystals. When partially stabilized tetragonal zirconia polycrystals (3Y-TZP) are exposed to hydrothermal conditions for relatively long periods, tetragonal to monoclinic phase transformation can occur (Ref. 14). Through this phase transformation, the strain associated with the transformation in the depth direction will be accommodated by grain boundary microcracking. This microcracking along the grain boundary is known to be responsible for porosity formation. Additional research, however, should be conducted to show if this grain boundary microcracking mechanism assisted by the stress-induced transformation in the hydrothermal degradation of 3Y-TZP can be applied to the case of zirconium alloy cladding oxidation.

The hydrothermal degradation of 3Y-TZP gives another insight into Zr alloy oxidation from the perspective of the diffusion element in the oxide. It is generally accepted that water species in the form of OH^- ions diffuse into material during the hydrothermal degradation of 3Y-TZP (Ref. 15~18). Guo conducted a good review of this process (Ref. 19).

Studies on Zr alloy corrosion have also suggested the presence and role of hydroxyl ion in oxide. Sundell showed that significant fractions of the boundaries were decorated with hydroxide (Ref. 20). Local reduction occurs and gaseous H_2 evolves on these hydroxide grain boundaries (Ref. 21). In this regard, a more detailed porosity formation and hydrogen pick-up mechanism has been proposed (Ref. 22, 23). Water species penetrate through the grain boundary of monoclinic ZrO_2 in the form of hydroxide. At the same time, hydrogen is generated by the cathodic reaction at the interface between the defect-free monoclinic ZrO_2 and the inner defect-rich tetragonal ZrO_2. The generated hydrogen, then, assists the aggregation of neutral oxygen vacancies. It is concluded that the porosity formed due to the aggregation of neutral oxygen vacancies (Ref. 22, 23). Finally, it is proposed that such pore formation allows the catastrophic unwanted permeation of hydrogen into the alloys prior to the breakdown of the barrier oxide (Ref. 22, 23). Therefore, the avalanche in the hydrogen pick-up fraction was taken to reflect pore formation (Ref. 22).

Thus, the various formation processes of porosity resulting from OH^- ion diffusion have some significant implications for the effects of the high hydrogen condition (50 cc/kg). If the OH^- ion was a diffusion element causing corrosion, the H_2 concentration of the water did not affect the OH^- ion concentration. Therefore, the water chemistry condition that simply increased the hydrogen concentration from 30 to 50 cc/kg may not have contributed to the formation of interlinked porosity through OH^- ion diffusion. Therefore it is expected that there will be no significant change in the high hydrogen concentration (50 cc/kg) condition even after the transition. In the case of Zn injection condition (30 ppb), it is also expected that there will be no significant difference because Zn does not contribute to porosity formation either.

V. Irradiation effect

If water molecules are dissociated by radiolysis, OH concentration will be increased. It may contribute to the formation of porosity and possibly affect the corrosion of the oxide layer. However, it is unclear whether this behavior occurs under 30 ppb Zn injection or 50 cc/kg high hydrogen conditions.

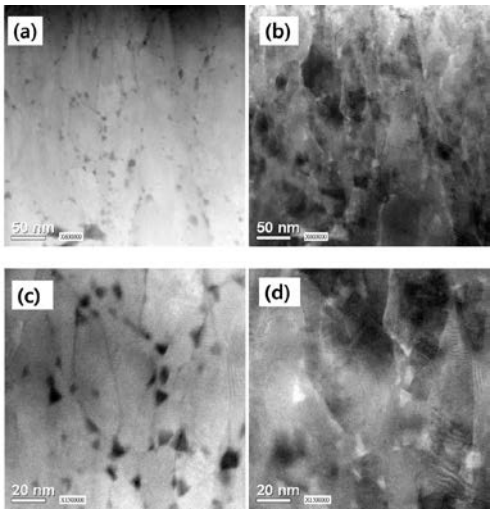

Fig. 2 (a) (c) Dark field STEM image of an area in the outer part of oxide showing the interlinked porosity. (b) (d) is Bright field STEM image of (a) (c).

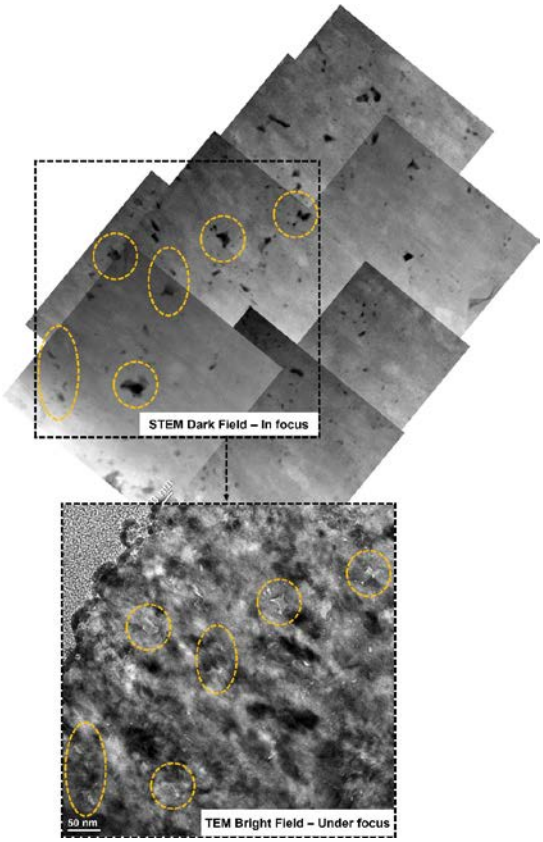

Fig. 3 Comparison of the STEM image (Dark field) and the TEM under-focusing image (Bright field) at the same locations for the 100 days corroded- sample in Zn injection condition (Orange circles indicate the same location).

IV. Conclusions

Microscopic examinations by CS-corrected STEM, TEM, SEM were conducted to characterize the oxide formed on samples oxidized in various water chemistry conditions. The main conclusions are as follows:

- There was no noticeable microstructural change in oxide formed Zr-Nb-Sn alloy samples with respect to the change in Zn or dissolved hydrogen concentration within the test duration of 100 days (pre-transition stage).
- Based on the comparison results of the oxide thicknesses of the samples corroded for 300 hours, 50 days, and 100 days in all water chemistry conditions, the 30-ppb Zn injection or increase of hydrogen from 30 to 50 cc/kg conditions did not significantly affect the oxide growth kinetics.
- Porosity along the oxide grain boundaries was analyzed using the TEM under-focusing technique indicating actual porous characterization. The porosity observed in the STEM dark-field image was also observed in the TEM under-focusing image, and the density of porosity decreased towards the metal/oxide interface.
- The interlinked porosity formed at the water/oxide interface widened when the porous region expanded in the metal/oxide interface direction as the oxide layer was corroded.
- From the perspective of OH- ion diffusion and pore formation, the absence of any noticeable effects of Zn injection suggests that Zn was not involved in the porosity formation process. Similarly, it is unlikely that the increase in dissolved hydrogen concentration can affect the porosity formation at least within the range of the experimental conditions we tested.

ACKNOWLEDGMENTS

This work was supported by the Korea Institute of Energy Technology Evaluation and Planning (KETEP) and the Ministry of Trade, Industry & Energy (MOTIE) of the Republic of Korea (No. 20168540000030), “Human Resources Program in Energy Technology” of the KETEP, granted financial resource from the MOTIE, Republic of Korea. (No. 20164010201000).

REFERENCES

1. T. R. Allen, R. J. M. Konings, and A. T. Motta, “5.03 corrosion of zirconium alloys”, *Comprehensive Nuclear Materials*, 49-68, (2012).
2. N. Ni *et al.*, “How the crystallography and nanoscale chemistry of the metal/oxide interface develops during the aqueous oxidation of zirconium cladding alloys”, *Acta Materialia*, **60**, 7132-7149 (2012).
3. P. Bossis, G. Lelievre, P. Barberis, X. Iltis, and F. LeFebvre, "Multi-Scale Characterisation of the Metal-Oxide Interface of Zirconium Alloys." In *12th Internation Symposium on Zr in the Nuclear Industry*, (2000).
4. B. Cox, “Some thoughts on the mechanisms of in-reactor corrosion of zirconium alloys”, *Journal of Nuclear Materials* **336,** 331–368, (2005).
5. W. Gong, H. Zhang, C. Wu, H. Tian and X. Wang, “The role of alloying elements in the initiation of nanoscale porosity in oxide films formed on zirconium alloys”, *Corrosion Science* **77**, 391-396, (2013).
6. A. T. Motta, A. Couet and R. J. Comstock, “Corrosion of Zirconium Alloys Used for Nuclear Fuel Cladding”, *Annual Review of Materials Research*, **45**, 311-343, (2015).
7. C. C. Lin, “A review of corrosion product transport and radiation field buildup in boiling water reactors”, *Progress in Nuclear Energy*, **51**, 207-224, (2009).
8. E. Chajduk and A. Bojanowska-Czajka, “Corrosion mitigation in coolant systems in nuclear power plants”, *Progress in Nuclear Energy*, **88**, 1-9, (2016).

9. J. S. Choi, S. C. Park, K. R. Park, H. Y. Yang, and O. B. Yang, "Effect of zinc injection on the corrosion products in nuclear fuel assembly", *Natural Science*, **05**, 173-181, (2013).
10. Electric Power Research Institute (EPRI). Pressurized Water Reactor Primary Water Chemistry Guidelines: Volume 1, Revision 5, EPRI, Palo Alto, CA: 2003. 1002884.
11. J. Wei *et al.*, "The effect of Sn on autoclave corrosion performance and corrosion mechanisms in Zr–Sn–Nb alloys", *Acta Materialia*, **61**, 4200-4214, (2013).
12. M. Ruhle and M. Wilkens, "Defocusing contrast of cavities I. Theory", *Cryst. Lattice Defects*, **6,** 129–140 (1975).
13. N. Ni *et al.*, "Porosity in oxides on zirconium fuel cladding alloys, and its importance in controlling oxidation rates", *Scripta Materialia*, **62**, 564-567, (2010).
14. J. Chevalier, L. Gremillard and S. Deville, "Low-Temperature Degradation of Zirconia and Implications for Biomedical Implants", *Annual Review of Materials Research*, **37**, 1-32, (2007).
15. J. A. Muñoz-Tabares, E. Jiménez-Piqué, and M. Anglada, "Subsurface evaluation of hydrothermal degradation of zirconia" *Acta Materialia*, **59**, 473-484, (2011).
16. H. Tsubakino, Y. Kuroda and M. Niibe, "Surface Relief Associated with Isothermal Martensite in Zirconia–3-mol%-Yttria Ceramics Observed by Atomic Force Microscopy", *Journal of the American Ceramic Society*, **82**, 2921-2923, (1999).
17. H. Tsubakino, K. Sonoda and R. Nozato, "Martensite transformation behaviour during isothermal ageing in partially stabilized zirconia with and without alumina addition", *Journal of Materials Science Letters*, **12**, 196-198, (1993).
18. W. Z. Zhu, T. C. Lei, & Y. Zhou, "Time-dependent tetragonal to monoclinic transition in hot-pressed zirconia stabilized with 2 mol % yttria", *Journal of Materials Science*, **28,** 6479–6483, (1993).
19. X. Guo, "Property degradation of tetragonal zirconia induced by low-temperature defect reaction with water molecules", *Chemistry of Materials*, **16,** 3988–3994, (2004).
20. G. Sundell, M. Thuvander, A. K. Yatim, H. Nordin and H. O. Andrén, "Direct observation of hydrogen and deuterium in oxide grain boundaries in corroded Zirconium alloys", *Corrosion Science*, **90**, 1-4, (2015).
21. G. Sundell, M. Thuvander, and H. O. Andrén, "Barrier oxide chemistry and hydrogen pick-up mechanisms in zirconium alloys", *Corrosion Science*, **102**, 490-502, (2016).
22. M. Lindgren, and I. Panas, "On the fate of hydrogen during zirconium oxidation by water: effect of oxygen dissolution in α-Zr", *RSC Adv.*, **4**, 11050-11058, (2014).
23. M. Lindgren, C. Geers, and I. Panas, "Possible origin and roles of nano-porosity in ZrO 2 scales for hydrogen pick-up in Zr alloys", *Journal of Nuclear Materials*, **492**, 22-31, (2017).